

# Coherent Frequency-Selective Polarimeter for Polarization-Mode Dispersion Monitoring

I. Roudas, G. A. Piech, M. Mlejnek, Y. Mauro, D. Q. Chowdhury, *Member, IEEE*, and M. Vasilyev, *Member, IEEE*

**Abstract**—Frequency-selective polarimeters measure the state of polarization of the individual spectral components of a modulated optical signal. They can be used either as stand-alone measuring devices or as parts of adaptive polarization-mode dispersion (PMD) compensators. This paper presents a novel frequency-selective polarimeter based on coherent detection, which has superior accuracy compared to previously proposed direct detection-based counterparts. This is due to the high-frequency resolution and power sensitivity of coherent detection, features that minimize the systematic and random error, respectively, in the measurement of the state of polarization of the individual spectral components of the received optical signal. The accuracy of the measurement is independent of the received signal bit rate and modulation format. The proposed frequency-selective polarimeter is studied both theoretically and experimentally. The primary theoretical contribution of this paper is a unified formalism, which allows the modeling of both direct and coherent detection-based frequency-selective polarimeters. Analytical expressions for the output signal of both types of frequency-selective polarimeters are derived. Based on these expressions, a common algorithm is proposed for the evaluation of the Stokes parameters. In addition, an example error signal is used as a metric in order to test the agreement of the theoretical model with the experimental measurements. The successful operation of the coherent frequency-selective polarimeter is demonstrated experimentally for a 10-Gb/s intensity-modulated nonreturn-to-zero (NRZ) optical signal in the presence of first-order polarization-mode dispersion. There is an excellent agreement between theory and experiment.

**Index Terms**—Coherent detection, polarization-mode dispersion (PMD) compensation, polarization-mode dispersion (PMD) monitoring.

## I. INTRODUCTION

**P**OLARIZATION-MODE dispersion (PMD) [1] limits the capacity of the majority of deployed optical fibers. In order to overcome this limitation, several optical and electronic adaptive PMD compensators have been proposed (see, e.g., [2] and the references therein). These compensators universally contain some form of PMD-monitoring device. These devices generate a feedback signal (in the following, referred to as *error signal*), which is used for driving the control unit of adaptive PMD compensators.

Several attributes of the received optical signal, which are affected by the presence of birefringence in the link, can be used for PMD monitoring. For example, a well-known manifestation of PMD is the variation of the state of polarization (SOP) along the spectrum of the received modulated optical signal, for fixed transmitted SOP [1]. Visualized in Stokes space, the received SOP traces a curve on the Poincaré sphere as a function of frequency. In principle, the shape, handedness, and length of the trajectory can all provide information about the PMD in the system.

This is the motivating factor for several proposed PMD-monitoring devices that measure the SOP of the individual spectral components of the received optical signal [3]–[6], [27]. In the following, we will refer to such devices as *frequency-selective polarimeters*. Conventional commercially available polarimeters, which cannot frequency resolve the SOP of a modulated signal but measure instead the degree of polarization (DOP), can be considered as a special case of frequency-selective polarimeters with low resolution.

In addition to their use in adaptive PMD compensators, frequency-selective polarimeters can be also used as stand-alone PMD measuring devices, in order to estimate the differential group delay (DGD) and the principal states of polarization (PSPs), in conjunction with standard PMD characterization techniques [4].

Frequency-selective polarimeters can be implemented using either direct [3]–[5] or coherent detection [6], [27]. In principle, these two detection methods provide identical functionality. However, it will be shown below that coherent frequency-selective polarimeters offer superior accuracy compared to their thermal noise-limited direct detection-based counterparts. This is due to the inherent high-frequency resolution (selectivity) and power sensitivity of coherent detection. These features minimize the systematic and random errors, respectively, in the measurement of the SOP of the individual spectral components of the received optical signal. This increase in measurement precision is achieved at the expense of an additional semiconductor laser (local oscillator).

This paper presents a detailed theoretical and experimental study of a novel frequency-selective polarimeter based on coherent detection, proposed recently by the authors [6], [27]. As a starting point, we develop a unified formalism that allows the modeling of both direct and coherent detection-based frequency-selective polarimeters. The formalism highlights the similarities and differences between both types of polarimeters. Analytical expressions for the output signal of both types of frequency-selective polarimeters are derived. Based on these expressions, a common algorithm is proposed for the evaluation

Manuscript received April 22, 2003; revised August 12, 2003.

I. Roudas was with Corning, Inc., Somerset, NJ 08873 USA. He is now with the Department of Electrical and Computer Engineering, University of Patras, Patras 26500, Greece (e-mail: roudas@ee.upatras.gr).

G. A. Piech, M. Mlejnek, Y. Mauro, and D. Q. Chowdhury are with Corning, Inc., Corning, NY 14831 USA.

M. Vasilyev was with Corning, Inc., Somerset, NJ 08873 USA. He is now with the Department of Electrical Engineering, University of Texas at Arlington, Arlington, TX 76019-0072 USA.

Digital Object Identifier 10.1109/JLT.2004.825234

of the Stokes parameters. Finally, the use of frequency-selective polarimeters as monitoring devices in adaptive PMD compensators is considered. An example error signal based on the variance of the frequency-resolved Stokes parameters is used as a metric to test the agreement between the theoretical model and the experimental measurements. Experimentally, the successful operation of the coherent frequency-selective polarimeter is demonstrated for a 10-Gb/s intensity-modulated nonreturn-to-zero (NRZ) optical signal in the presence of first-order polarization-mode dispersion. There is an excellent agreement between theory and experiment.

It is worth noting that all the above results are original since there is no previous technical literature on the subject apart from the initial papers [4], [6], [27]. However, we have borrowed elements from the formalism of digital coherent detection receivers [7] and spectral analysis [8]–[11].

The remainder of this paper is divided into three sections, namely theoretical model, experimental setup, and results and discussion. Section II is organized as follows. The operating principle of frequency-selective polarimeters is described in Section II-A and the unified model of frequency-selective polarimeters is outlined in Section II-B. The algorithm for the estimation of the Stokes parameters as a function of frequency is presented in Section II-C. Finally, in Section II-D, an analytical expression for an example error signal in the presence of first-order PMD is derived. The experimental setup used to test the coherent frequency-selective polarimeter is described in Section III. Section IV presents experimental results that demonstrate the successful operation of the coherent frequency-selective polarimeter. The details of the theoretical model are given in the Appendix.

## II. MODEL OF FREQUENCY-SELECTIVE POLARIMETERS

### A. Operating Principle

The operation of a frequency-selective polarimeter is similar to the operation of an optical spectrum analyzer [8].

In principle, an optical spectrum analyzer can be implemented using a tunable narrow-band optical filter and an optical power meter, composed of a quadratic detector (i.e., photodiode) and a low-pass electronic filter [8]. Successive power measurements corresponding to different center frequencies of the tunable narrow-band optical filter allow the scanning of the power spectral density (psd) of the received optical signal.

In practice, several different versions of this basic idea can be used for spectral analysis. For instance, one could use an array of narrow-band optical filters with equidistant fixed center frequencies in parallel, followed by an array of optical power meters. A practical implementation of this design uses a diffraction grating (instead of narrow-band optical filters in parallel) and a photodetector array. Another possibility would be to use coherent detection, in order to translate the optical signal psd in the microwave frequency domain, followed by an electronic narrow-band bandpass filter (BPF) and a microwave power meter, composed of a quadratic detector (i.e., microwave mixer) and a low-pass electronic filter (LPF) [9]–[11]. It is possible to scan the whole optical signal psd by changing the carrier frequency of the local oscillator of the coherent receiver.

A frequency-selective polarimeter is nothing more than an optical spectrum analyzer with the addition of a polarization-selective element before the photodetection. Therefore, all three aforementioned versions of optical spectrum analyzers have been used to implement frequency-selective polarimeters [3]–[6], [27]. The role of the polarization-selective element is performed by an optical polarizer, in the case of direct detection-based spectrum analyzers [3]–[5], and the combination of a local oscillator with a polarization transformer, in the case of a coherent detection-based spectrum analyzer [6], [27]. It will be shown below that successive power measurements with different polarizers in the former case and with different local oscillator SOPs in the latter case can be used to calculate the SOP of the individual spectral components of the received optical signal.

The operation of different types of direct detection-based frequency-selective polarimeters is explained in detail in [3]–[5]. Therefore, the rest of this section is devoted to the description of the architecture and the operation of the coherent frequency-selective polarimeter [6], [27].

Before proceeding further, it is worth noting that several coherent optical receiver architectures were proposed in the past for the detection of various digital modulation formats [7]. For that application, desirable characteristics of the coherent detection are its increased sensitivity and selectivity compared to the direct detection. On the other hand, the polarization sensitivity of the coherent detection is considered to be a drawback for all digital modulation formats and several methods have been proposed for its cancellation [7]. In contrast, in the current context, the coherent receiver is intended to be used as an analog measuring instrument of the SOP as a function of frequency. The data content of the received optical signal is discarded. To achieve these objectives, a novel coherent receiver architecture was proposed in [6] and [27]. Its rationale can be understood through comparison with the direct detection-based frequency-selective polarimeter proposed in [4].

Fig. 1(a) and (b) shows the block diagrams of the direct detection [4] and coherent detection-based frequency-selective polarimeters [6], [27], respectively. The direct detection-based frequency-selective polarimeter [Fig. 1(a)] is composed of a tunable optical filter (OF), a polarizer (P), a photodiode (PH), an electronic preamplifier (PA), and a low-pass filter (LPF). The coherent frequency-selective polarimeter [Fig. 1(b)] is composed of a local oscillator (LO); a polarization transformer (PT); an ideal, lossless, and polarization-independent 3-dB coupler; a balanced receiver front-end consisting of two identical p-i-n photodiodes (PH) and an electronic preamplifier (PA); a bandpass filter (BPF); and a square-law detector consisting of a microwave mixer and a low-pass filter (LPF).

There are direct analogies between the functionalities of the components of the frequency-selective polarimeters depicted in Fig. 1(a) and (b).

- 1) The tunable optical filter of Fig. 1(a) is functionally equivalent to the electronic BPF of Fig. 1(b).
- 2) The polarizer of Fig. 1(a) corresponds to the local oscillator and the polarization transformer of Fig. 1(b).
- 3) The photodiode and electronic LPF of Fig. 1(a) correspond to the square-law detector of Fig. 1(b).

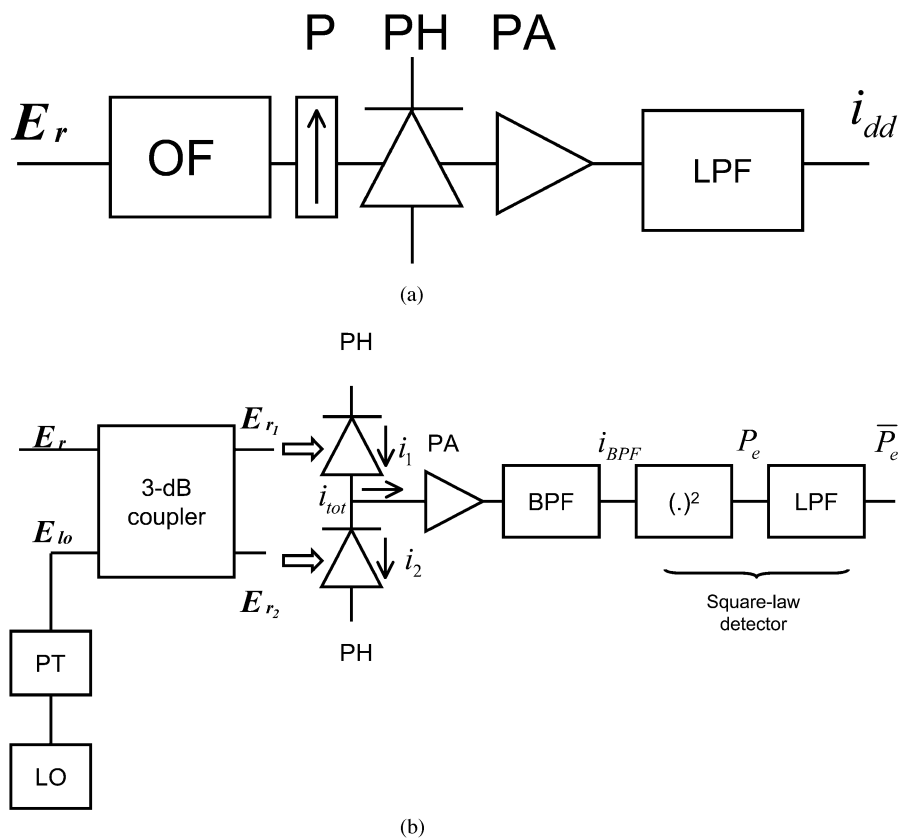


Fig. 1. (a) Schematic of a direct detection-based frequency-selective polarimeter [4]. OF = tunable optical filter, P = polarizer, PH = photodiode, PA = preamplifier, LPF = low-pass filter,  $\mathbf{E}_r$  = received electric field, and  $i_{dd}$  = output photocurrent. (b) Schematic of the proposed coherent frequency-selective polarimeter [6], [27]. LO = local oscillator, PT = polarization transformer, PH = photodiode, PA = preamplifier, BPF = band-pass filter,  $(\cdot)^2$  = square-law device (microwave mixer), LPF = low-pass filter,  $\mathbf{E}_r$  = received electric field,  $\mathbf{E}_{lo}$  = local oscillator electric field after the polarization transformer,  $\mathbf{E}_{r_{1,2}}$  = electric fields at the output ports of an ideal lossless 3-dB coupler,  $i_{1,2}$  = photocurrents at the two branches of the balanced receiver,  $i_{tot}$  = total photocurrent,  $i_{BPF}$  = photocurrent at the output of the BPF,  $P_e$  = instantaneous electrical power, and  $\bar{P}_e$  = output signal of the coherent frequency-selective polarimeter.

The role of the 3-dB coupler and the balanced receiver front end of Fig. 1(b) is simply to perform a frequency translation of the received optical signal psd to the microwave frequency domain (see below). There is no homologous functionality in the direct detection-based frequency-selective polarimeter depicted in Fig. 1(a). Apart from this difference, the two frequency-selective polarimeters are functionally equivalent. It is worth noting that the reversal of order between cutting a spectral slice and selecting a specific SOP in Fig. 1(a) and (b) has no consequence in the measurement, since both operations are linear.

A full mathematical analysis of the coherent frequency-selective polarimeter is given in the Appendix. A qualitative understanding of its operation can be gained from Fig. 2. The received two-sided optical signal psd is shown in Fig. 2(a) [curves (1)]. The signal power is concentrated around the signal carrier frequency  $\pm f_s$ . The psd of the local oscillator is also depicted as two discrete spectral lines at the local oscillator carrier frequency  $\pm f_{lo}$  [curves (2)]. Coherent detection downshifts the received optical signal psd around  $\pm f_{IF}$ , where  $f_{IF}$  is the intermediate frequency defined as  $f_{IF} \equiv f_s - f_{lo}$  [curves (4) in Fig. 2(b)]. The downshifted psd is scaled by a multiplication factor, which is a function of the alignment of the signal and local oscillator SOPs

[curves (3) in Fig. 2(a)].<sup>1</sup> A BPF is used to cut a narrow (ideally infinitesimal) slice of the intermediate frequency signal psd around the BPF center frequency  $f_c$ . The squared module of the transfer function of the BPF is depicted as shaded areas in Fig. 2(b) [curves (5)]. Due to the finite BPF bandwidth  $B_{BPF}$ , the signal at the output of the BPF is not a pure sinusoid with frequency  $f_c$ , but has amplitude modulation resulting from the presence of spectral components adjacent to the BPF center frequency  $f_c$ . This amplitude modulation creates fluctuations at the output of the coherent frequency-selective polarimeter (referred to in the following as *data noise*). The rest of the receiver is used to measure the average electrical power at the output of the BPF. For this purpose, the signal first passes through a microwave mixer, which is assumed to be an ideal square-law device. The signal at the output of the microwave mixer is the instantaneous electrical power consumed by the microwave photocurrent at the output of the BPF on a unit resistor. It is comprised of spectral components around the frequencies  $f = 0$  and  $\pm 2f_c$  [curves (6) in Fig. 2(c)]. The purpose of the LPF is two-fold: 1) to eliminate the higher harmonic at  $\pm 2f_c$  at the output of the microwave mixer and 2) to average the ampli-

<sup>1</sup>The balanced receiver front end also introduces thermal and shot noise. These noises, as well as the phase noises of the transmitter and local oscillator, are omitted from Fig. 2 in order to avoid clutter.

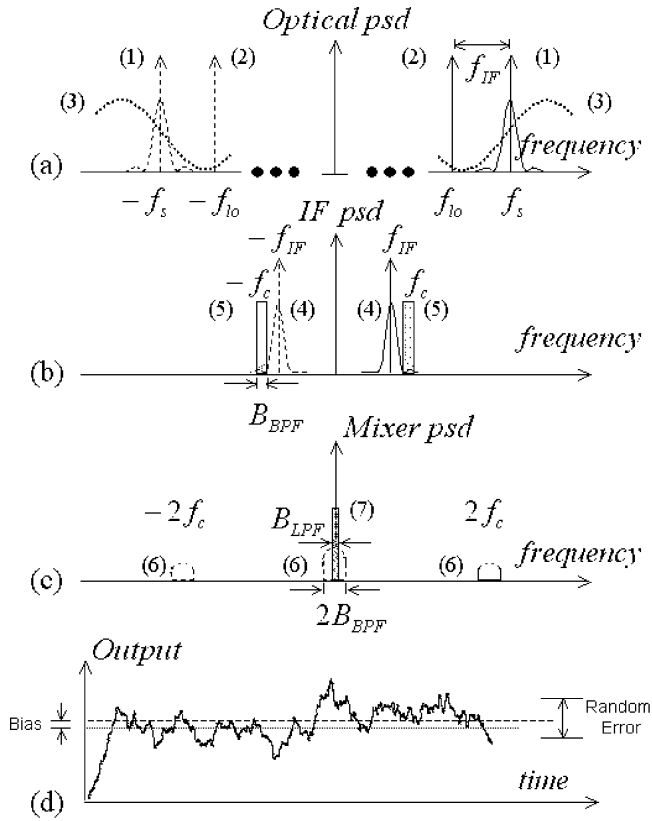


Fig. 2. Qualitative explanation of the operating principle of the proposed coherent frequency-selective polarimeter, as interpreted from (28)–(41) in the Appendix. (a) Received optical signal psd [curves (1)], local oscillator psd [curves (2)], and multiplication factor introduced by the coherent detection [dotted lines (3)]. (b) Intermediate-frequency psd [curves (4)] and squared module of the transfer function of the BPF (shaded area) [curves (5)]. (c) The psd at the output of the microwave mixer [curves (6)] and squared module of the LPF transfer function (shaded area) [curve (7)]. (d) Signal waveform at the output of the LPF, actual mean (dashed line), and true average value (dotted line). Solid-line psds are centered at positive frequencies, broken-line psds are centered at negative frequencies.  $f_s$  = signal carrier frequency,  $f_{lo}$  = local oscillator carrier frequency,  $f_{IF}$  = intermediate frequency,  $f_c$  = BPF center frequency,  $B_{BPF}$  = BPF equivalent noise bandwidth,  $B_{LPF}$  = LPF equivalent noise bandwidth. Conditions: First-order PMD with DGD  $\tau = 1/(10R_b)$ , ideal NRZ signal, absence of spectral folding and phase, thermal, and shot noises.

tude variations of the instantaneous electrical power due to the data, shot, thermal, and phase noise after the BPF. The squared module of the LPF transfer function is depicted as a shaded area in Fig. 2(c) [curve (7)]. Due to the finite LPF bandwidth  $B_{LPF}$ , the output signal has residual modulation resulting from the spectral components around the direct current (dc) [Fig. 2(c)]. In other words, the averaging performed by the LPF is not perfect, so the output of the coherent frequency-selective polarimeter varies over time [Fig. 2(d)]. Therefore, the measurement performed by the coherent frequency-selective polarimeter signal is not exactly equal to the average electrical power at the output of the BPF (dotted line), but has noise (referred to in the following as *random error*) [Fig. 2(d)]. The noise variations can be reduced by decreasing the BPF, LPF bandwidths  $B_{BPF}$ ,  $B_{LPF}$  at the expense of the measurement time. There is also a certain deterministic deviation of the mean of the output signal (dashed line) from the true value of the average electrical power (dotted line) [Fig. 2(d)]. This offset is referred to in the following as *sys-*

*tematic* (or *bias*) error [8], [12]. The systematic error has double origin: 1) the variation of the received signal SOP within the BPF bandwidth and 2) the average electrical power of the shot and thermal noise within the BPF bandwidth. It can be reduced by decreasing the BPF bandwidth.

The measurement of the average electrical power is repeated for four distinct local oscillator SOP settings. If the local oscillator SOP settings are selected appropriately, as explained in Section II-C, the results of these measurements can be combined to estimate the Stokes parameters of the spectral components at a distance  $f_c - f_{IF}$  from the psd center. In order to estimate the received signal SOP at different frequencies, the intermediate frequency is successively changed by tuning the carrier frequency of the local oscillator. At each new value of the intermediate frequency  $f_{IF}$ , a different slice of the psd at a distance  $f_c - f_{IF}$  from the psd center is scanned across the BPF and the measurement procedure is repeated.

In the previous qualitative analysis, it was implicitly assumed that the received optical signal psd is strictly band-limited with spectral occupancy  $B$  and that the BPF center frequency  $f_c$  is larger than  $(B + B_{BPF})/2$ . This condition is necessary in order to avoid overlap of the tails of the psd segments centered at  $\pm f_{IF}$  within the BPF passband for all measurements (referred to in the following as *spectral folding* [13]). In practice, however, the optical signal psd is not strictly band-limited, but extends to infinity. Therefore, spectral folding cannot be avoided. Nevertheless, the psd of the modulated optical signal decreases rapidly away from  $\pm f_{IF}$  and becomes negligible at a distance a few times the bit rate, depending on the modulation format. Therefore, if the BPF center frequency  $f_c$  was sufficiently high compared to the bit rate  $R_b$ , i.e.,  $f_c \gg R_b$ , there would be no significant spectral folding and the previous analysis would hold.

However, the choice of the BPF center frequency is dictated by the cost of the balanced receiver front-end and the electronic parts of the coherent frequency-selective polarimeter. To reduce this cost, a low BPF center frequency compared to the bit rate is chosen, i.e.,  $f_c \ll R_b$ . This requirement implies that significant spectral folding occurs. An example of spectral folding is shown in Fig. 3(b). Two spectral slices, at a distance  $f_{IF} - f_c$  from  $f_{IF}$  (solid line) and  $f_{IF} + f_c$  from  $-f_{IF}$  (dashed line), respectively, pass simultaneously through the passband of the BPF centered at  $f_c$  (shaded area). Similarly, two other spectral slices, at a distance  $f_{IF} - f_c$  from  $-f_{IF}$  (dashed line) and  $f_{IF} + f_c$  from  $f_{IF}$  (solid line), respectively, pass simultaneously through the complex conjugate passband of the BPF centered at  $-f_c$  (shaded area). Experimental results in Section IV indicate that one has the right to add the solid and dashed lines (see Figs. 6–9 and the discussion in the Appendix). Consequently, it is conjectured that the mean value of the signal at the output of the coherent frequency-selective polarimeter is a function of the SOPs of the received optical signal spectral components at  $f_{IF} \pm f_c$ , weighted by the received optical signal psd values at  $f_{IF} \pm f_c$  [see (4)]. If the SOPs of the received optical signal components at  $f_{IF} \pm f_c$  do not differ substantially, the qualitative analysis of Fig. 2 holds. There is no need for image-frequency rejection [14]–[16].

There is an important remark regarding the coherent receiver terminology: Coherent receivers are characterized as *homodyne*

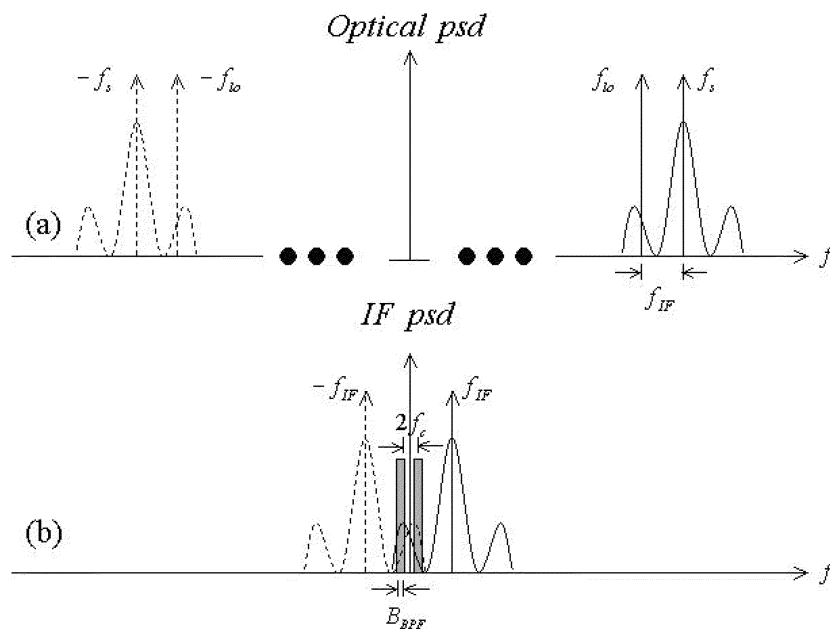


Fig. 3. Example of spectral folding. (a) Received optical signal and local oscillator psd. (b) IF psd and squared module of the transfer function of the BPF (shaded area). The tails of the psd segments centered at  $\pm f_{IF}$  overlap within the BPF passbands centered at  $\pm f_c$  (denoted by shaded rectangles). Conditions: absence of PMD, exaggerated secondary lobes of the received signal PSD compared to the NRZ modulation psd, for easy visualization. Symbols are the same as in Fig. 2.

if the intermediate frequency is zero and as *heterodyne* otherwise [17]. In the case of the proposed coherent frequency-selective polarimeter, in order to measure the variation of the Stokes parameters of the received optical signal within a frequency interval  $\Delta f$  (referred to in the following as *scanning range*), the intermediate frequency is successively varied in the interval  $[f_c - \Delta f/2, f_c + \Delta f/2]$  by tuning the local oscillator carrier frequency. For PMD monitoring applications, the scanning range  $\Delta f$  is comparable to the spectral occupancy of the signal.<sup>2</sup> Assuming  $f_c \ll R_b$  to minimize the cost of the electronic parts of the receiver, the operation of the proposed coherent frequency-selective polarimeter changes from homodyne (i.e.,  $f_{IF} = 0$  for the measurement of the Stokes parameters at a distance  $f_c$  from the psd center) to heterodyne (for measurements at all other frequencies). Therefore, the generic term “coherent” is used to describe the proposed frequency-selective polarimeter.

Finally, it is worth emphasizing that there are three architectural differences between the proposed coherent frequency-selective polarimeter and the conventional digital coherent receivers. First, notice that, in the former device, the intermediate frequency does not coincide with the BPF center frequency, except for the measurement of the Stokes parameters of the spectral components at the psd center. In the latter devices,  $f_c = f_{IF}$  always. Second, in the proposed coherent frequency-selective polarimeter  $f_c \ll R_b$ , whereas in conventional digital coherent receivers  $f_c \gg R_b$ , at least in principle. Third, in the proposed coherent frequency-selective polarimeter  $B_{BPF} \ll R_b$ , whereas in conventional digital coherent receivers  $B_{BPF} \sim R_b$ .

<sup>2</sup>The spectral occupancy (bandwidth) of not strictly band-limited signals is arbitrarily defined as the frequency range within which a certain percentage of the signal power is confined [18]. For instance, for NRZ modulation, the 95% spectral occupancy is  $B = 3R_b$  [19].

## B. Mathematical Formalism

The Appendix presents a unified model of the frequency-selective polarimeters shown in Fig. 1. Analytical expressions for the output signal of both types of frequency-selective polarimeters are derived. In this section, only the final results are reported.

We distinguish two different received optical signal types, namely, monochromatic continuous waves (CWs) and stochastic signals. The second signal type is of practical interest because it encompasses all modulation formats. Nevertheless, it is instructive to first study the simplified case of CW signals. In the remainder of this section, all transmitter, local oscillator, and receiver noises are neglected.

1) *CW Signals*: When the received optical signal is a plane monochromatic wave, the output signal of the coherent frequency-selective polarimeter is [see (26)]

$$\bar{P}_e = 2R^2 P_r P_{lo} |\langle e_{lo} | e_r \rangle|^2 \quad (1)$$

where  $\bar{P}_e$  is the average electrical power on a unit resistor,  $R$  is the responsivity of both photodiodes at the two branches of the balanced receiver,  $P_r$  is the average power of the received optical signal,  $P_{lo}$  is the average power of the local oscillator at the output of the polarization transformer,  $|e_r\rangle$  is a normalized Jones vector denoting the SOP of the received optical signal, and  $|e_{lo}\rangle$  is a normalized Jones vector denoting the SOP of the local oscillator at the output of the polarization transformer.

Expression (1) shows that, in the absence of noise, the signal at the output of the coherent frequency-selective polarimeter is proportional to the average optical powers  $P_r$ ,  $P_{lo}$  of the received signal and local oscillator, respectively, and to the squared modulus of the inner product between the Jones vectors of the received signal and the local oscillator.

It is straightforward to show that the photocurrent at the output of the frequency-selective polarimeter based on direct detection shown in Fig. 1(a) is given by a similar expression [see (27)]

$$i_{\text{dd}} = RP_r |\langle e_{\text{pol}} | e_r \rangle|^2 \quad (2)$$

where  $|e_{\text{pol}}\rangle$  is a normalized Jones vector denoting the eigenaxis of the polarizer.

By comparing (1) and (2), we conclude that the operation of both types of frequency-selective polarimeters is equivalent. However, in the case of frequency-selective polarimeters based on coherent detection, there is amplification of the received signal, with the amount of amplification being proportional to the average power of the local oscillator  $P_{\text{lo}}$ . This amplification factor leads to higher electrical signal-to-noise ratio (ESNR) and, hence, to smaller relative random error in the measurement of the SOP of the individual spectral components of the received optical signal.

2) *Stochastic Signals*: Consider that the electric field of the received optical signal is modulated by a random signal with complex envelope  $\tilde{g}(t)$  with unit power.

In the absence of spectral folding, the expected value of the output signal of the coherent frequency-selective polarimeter is [see (41)]

$$E \{ \bar{P}_e(t) \} \cong 2R^2 P_r P_{\text{lo}} |\langle e_{\text{lo}} | e_r(f_c - f_{\text{IF}}) \rangle|^2 \times \Phi_{\tilde{g}}(f_c - f_{\text{IF}}) B_{\text{BPF}} \quad (3)$$

where  $E\{\cdot\}$  denotes expected value (ensemble average),  $\Phi_{\tilde{g}}(f)$  is the psd of  $\tilde{g}(t)$ , and  $B_{\text{BPF}}$  is the BPF equivalent noise bandwidth defined as [20]

$$B_{\text{BPF}} \equiv \frac{\int_{-\infty}^{\infty} |\tilde{H}_{\text{BPF}}(f)|^2 df}{|\tilde{H}_{\text{BPF}}(0)|^2}$$

where  $\tilde{H}_{\text{BPF}}(f)$  is the low-pass equivalent representation of the BPF transfer function.

It is observed that (1) and (3) are essentially the same, with the exception of the substitution of the average received signal power  $P_r$  by  $P_r \Phi_{\tilde{g}}(f_c - f_{\text{IF}}) B_{\text{BPF}}$ , which is the fraction of the average received signal power contained within the BPF bandwidth.

In the presence of spectral folding, experimental results in Section IV (see Fig. 6–9) indicate that the expected value of the output signal of the coherent frequency-selective polarimeter is similar to (3)

$$\begin{aligned} E \{ \bar{P}_e(t) \} &\cong 2R^2 P_r P_{\text{lo}} B_{\text{BPF}} \\ &\times \left[ |\langle e_{\text{lo}} | e_r(f_c - f_{\text{IF}}) \rangle|^2 \Phi_{\tilde{g}}(f_c - f_{\text{IF}}) \right. \\ &\left. + |\langle e_{\text{lo}} | e_r(-f_c - f_{\text{IF}}) \rangle|^2 \Phi_{\tilde{g}}(-f_c - f_{\text{IF}}) \right]. \quad (4a) \end{aligned}$$

Assuming that expression (4a) holds in all cases of practical interest and that the SOPs of the received optical signal spectral components at  $\pm f_c - f_{\text{IF}}$  do not differ substantially, the expected

value of the output signal of the coherent frequency-selective polarimeter can be written as

$$E \{ \bar{P}_e(t) \} \cong 2R^2 P_r P_{\text{lo}} B_{\text{BPF}} |\langle e_{\text{lo}} | e_r(-f_{\text{IF}}) \rangle|^2 \times [\Phi_{\tilde{g}}(f_c - f_{\text{IF}}) + \Phi_{\tilde{g}}(-f_c - f_{\text{IF}})]. \quad (4b)$$

It is observed that (3) and (4b) are essentially the same, apart from the substitution of  $\Phi_{\tilde{g}}(f_c - f_{\text{IF}})$  by  $\Phi_{\tilde{g}}(f_c - f_{\text{IF}}) + \Phi_{\tilde{g}}(-f_c - f_{\text{IF}})$ .

The expected value of the photocurrent at the output of frequency-selective polarimeters based on direct detection is given by a similar expression [see (42)] as

$$E \{ i_{\text{dd}}(t) \} \cong RP_r |\langle e_{\text{pol}} | e_r(f_c - f_s) \rangle|^2 \Phi_{\tilde{g}}(f_c - f_s) B_o \quad (5)$$

where  $B_o$  is the equivalent noise bandwidth of the tunable optical filter.

For the derivation of (3)–(5), it was assumed that the terms  $|\langle e_{\text{lo}} | e_r(\pm f - f_{\text{IF}}) \rangle|^2$ ,  $|\langle e_{\text{pol}} | e_r(f - f_s) \rangle|^2$ ,  $\Phi_{\tilde{g}}(\pm f - f_{\text{IF}})$ , and  $\Phi_{\tilde{g}}(f - f_s)$  do not vary significantly within the passband of the BPF (of the coherent frequency-selective polarimeter) and the tunable optical filter (of the direct detection-based frequency-selective polarimeter), respectively. This assumption is not strictly valid in the case of direct detection-based frequency-selective polarimeters, because practical tunable optical filters have wide bandwidths ( $\sim$  GHz). This leads to higher systematic error in the case of direct detection-based frequency-selective polarimeters (see the discussion in the Appendix).

### C. Algorithm for the Evaluation of Stokes Parameters

Due to the similarity between (1)–(3), (4b), and (5), it is possible to use the same algorithm for the evaluation of the Stokes parameters for coherent and for direct detection-based frequency-selective polarimeters.

The algorithm is well-known (see, e.g., [21]), but it is formally rederived here in order to emphasize that four *arbitrary, noncoplanar* (in Stokes space) settings of the local oscillator SOP (in the case of the proposed coherent frequency-selective polarimeter), or polarizers (in the case of direct detection-based frequency-selective polarimeters) can be used for the evaluation of the Stokes parameters of the received signal.<sup>3</sup>

For the formal description of the algorithm, (1) is used for simplicity. The adaptation of the algorithm in the case of (2), (3), (4b), and (5) is trivial.

As a starting point, it is convenient to express the inner product in Jones space as a function of the inner product in Stokes space (see [23, relation (3.11)])

$$|\langle e_{\text{lo}} | e_r \rangle|^2 = \frac{1}{2} (1 + \hat{e}_{\text{lo}} \hat{e}_r) \quad (6)$$

where  $\hat{e}_r$ ,  $\hat{e}_{\text{lo}}$  are the normalized Stokes vectors corresponding to the received signal and local oscillator SOPs, respectively.

Substituting (6) into (1), the average electrical power at the output of the coherent frequency-selective polarimeter is

$$\bar{P}_e = R^2 P_r P_{\text{lo}} (1 + \hat{e}_r \hat{e}_{\text{lo}}). \quad (7)$$

<sup>3</sup>An alternative algorithm for the evaluation of the Stokes parameters was proposed by [22].

By substituting the Cartesian coordinates of  $\hat{e}_r, \hat{e}_{l_0}$  in (7), the average electrical power at the output of the coherent frequency-selective polarimeter, corresponding to the  $k$ th local oscillator SOP, may be

$$\bar{P}_e|_k = R^2 P_r P_{l_0} \left( 1 + S_x S_x^{(k)} + S_y S_y^{(k)} + S_z S_z^{(k)} \right) \quad (8)$$

where  $(S_x, S_y, S_z)$  are the normalized Stokes components of the received optical signal SOP  $\hat{e}_r$  and  $(S_x^{(k)}, S_y^{(k)}, S_z^{(k)})$  are the normalized Stokes components of the  $k$ th local oscillator setting  $\hat{e}_{l_0}^{(k)}$ .

Using (8), first it is possible to estimate the multiplicative factor  $R^2 P_r P_{l_0}$  from two measurements of the photocurrent corresponding to two antiparallel (in Stokes space) local oscillator SOPs as follows:

$$\bar{P}_e|_{(0)} = R^2 P_r P_{l_0} \left( 1 - S_x S_x^{(1)} - S_y S_y^{(1)} - S_z S_z^{(1)} \right) \quad (9a)$$

$$\bar{P}_e|_{(1)} = R^2 P_r P_{l_0} \left( 1 + S_x S_x^{(1)} + S_y S_y^{(1)} + S_z S_z^{(1)} \right) \quad (9b)$$

where we have used  $S_i^{(0)} = -S_i^{(1)}$  for the antiparallel Stokes vectors [23]. Adding (9a) and (9b) yields

$$R^2 P_r P_{l_0} = \frac{\bar{P}_e|_{(0)} + \bar{P}_e|_{(1)}}{2}. \quad (10)$$

It is then possible to evaluate the normalized Stokes parameters from two additional measurements of the photocurrent. For three noncoplanar in Stokes space (but not necessarily mutually orthogonal) local oscillator SOPs  $k = 1, 2, 3$ , (8) yields

$$\begin{aligned} \bar{P}_e|_{(1)} &= R^2 P_r P_{l_0} \left( 1 + S_x S_x^{(1)} + S_y S_y^{(1)} + S_z S_z^{(1)} \right) \\ \bar{P}_e|_{(2)} &= R^2 P_r P_{l_0} \left( 1 + S_x S_x^{(2)} + S_y S_y^{(2)} + S_z S_z^{(2)} \right) \\ \bar{P}_e|_{(3)} &= R^2 P_r P_{l_0} \left( 1 + S_x S_x^{(3)} + S_y S_y^{(3)} + S_z S_z^{(3)} \right) \end{aligned} \quad (11)$$

or, alternatively, in matrix form

$$\begin{pmatrix} S_x^{(1)} & S_y^{(1)} & S_z^{(1)} \\ S_x^{(2)} & S_y^{(2)} & S_z^{(2)} \\ S_x^{(3)} & S_y^{(3)} & S_z^{(3)} \end{pmatrix} \begin{pmatrix} S_x \\ S_y \\ S_z \end{pmatrix} = \frac{1}{R^2 P_r P_{l_0}} \begin{pmatrix} \bar{P}_e|_{(1)} \\ \bar{P}_e|_{(2)} \\ \bar{P}_e|_{(3)} \end{pmatrix} - 1. \quad (12)$$

If the three local oscillator SOPs are known, the signal Stokes parameters can be evaluated by

$$S = A^{-1} B \quad (13a)$$

where we defined

$$\begin{aligned} A &= \begin{pmatrix} S_x^{(1)} & S_y^{(1)} & S_z^{(1)} \\ S_x^{(2)} & S_y^{(2)} & S_z^{(2)} \\ S_x^{(3)} & S_y^{(3)} & S_z^{(3)} \end{pmatrix} \\ S &= \begin{pmatrix} S_x \\ S_y \\ S_z \end{pmatrix} \\ B &= \frac{1}{R^2 P_r P_{l_0}} \begin{pmatrix} \bar{P}_e|_{(1)} \\ \bar{P}_e|_{(2)} \\ \bar{P}_e|_{(3)} \end{pmatrix} - 1. \end{aligned} \quad (13b)$$

The simplest solution of the above set of equations is obtained for local oscillator settings  $k = 1, \dots, 3$ , corresponding to linear  $0^\circ$ ,  $45^\circ$  and right or left circular polarization (which makes the matrix  $A$  identity in a right or left circular Stokes space, respectively). However, as discussed in [24], the latter is not the optimal choice of local oscillator settings. A more robust polarimeter results if the four SOPs are as far apart on the Poincaré sphere as possible, which makes them the vertices of the maximum-volume tetrahedron inscribed inside the sphere.

For the practical implementation of the algorithm, a  $4 \times 4$  linear set of equations, derived from (8) for four arbitrary non-coplanar (in Stokes space) settings of the local oscillator SOP, is solved instead of (10) and (13).

In conclusion, the estimation of the Stokes parameters as a function of frequency involves three steps.

- 1) Tune the local oscillator to a series of closely spaced frequencies across the signal bandwidth.
- 2) At each frequency, change the local oscillator SOP between four known SOP settings and measure the corresponding average electrical powers at the output of the coherent frequency-selective polarimeter.
- 3) Solve a  $4 \times 4$  linear set of equations at each frequency.

Finally, it is worth noting that, in the most general case of spectral folding, (4a) must be used instead of (4b). Repeating the calculations (6)–(13), it is straightforward to show that the aforementioned algorithm leads to an average estimated signal Stokes vector  $\bar{\hat{e}}_r(f)$  as a function of frequency

$$\bar{\hat{e}}_r(f) \cong \frac{\hat{e}_r(f_c - f) \Phi_{\bar{g}}(f_c - f) + \hat{e}_r(-f_c - f) \Phi_{\bar{g}}(-f_c - f)}{\Phi_{\bar{g}}(f_c - f) + \Phi_{\bar{g}}(-f_c - f)}. \quad (14)$$

#### D. Example Error Signal

A major application of frequency-selective polarimeters is their use as PMD monitoring devices in adaptive PMD compensators. Therefore, a reasonable figure of merit for the estimation of their performance is the quality of the generated error signal.

Numerous error signals can be generated from the frequency-resolved Stokes parameters provided by frequency-selective polarimeters. The choice of the most adequate error signal form depends on several criteria, e.g., order of desired PMD compensation, monotonicity of the error signal as a function of power penalty in order to achieve a desired error probability, and so forth. The optimal choice of error signal lies outside of the scope of the present study.

In Section IV, an example error signal based on the variance of the frequency-resolved Stokes parameters is used as a metric to test the agreement between the theoretical model and the experimental measurements. Its formal definition is similar to the one proposed by [3] (with the exception of a square root difference)

$$\varepsilon = \left\langle |\hat{e}_r(\omega) - \langle \hat{e}_r(\omega) \rangle|^2 \right\rangle \quad (15)$$

where the angled brackets denote spectral average across the desired scanning range  $\Delta f$  using an arbitrary weighting function.<sup>4</sup>

To illustrate the monotonicity and the range of values of (15), we may consider the case of an optical signal passing through a polarization-maintaining (PM) fiber with slow eigenaxis  $\hat{e}_f$ , which introduces DGD equal to  $\tau$ . For an input signal with fixed SOP  $\hat{e}_s$ , the output SOP varies as a function of frequency [23]

$$\hat{e}_r(\omega) = \cos(\omega\tau)\hat{e}_s + [1 - \cos(\omega\tau)](\hat{e}_s\hat{e}_f)\hat{e}_f + \sin(\omega\tau)\hat{e}_f \times \hat{e}_s \quad (16)$$

which is valid in a right circular Stokes space [23].

By substituting the Cartesian coordinates of  $\hat{e}_s, \hat{e}_f$  in (16), a general expression for the normalized Stokes components of the received optical signal SOP can be derived as

$$S_k(\omega) = \alpha_k + \beta_k \cos(\omega\tau + \theta_k), k = x, y, z \quad (17)$$

where  $\alpha_k, \beta_k, \theta_k, k = x, y,$  and  $z$  are interdependent constants, which can be calculated analytically, but their expressions are cumbersome and are omitted here.

Expression (17) is a formal proof of the well-known fact that after transmission through a birefringent device with first-order PMD, the locus of the output signal SOP in Stokes space traces a circle on the Poincaré sphere as a function frequency and, consequently, the corresponding Stokes parameters vary sinusoidally.

A closed-form expression for the error signal in the presence of first-order PMD can be derived by substituting (16) into (15) and performing the spectral averages, assuming a uniform weighting function  $1/(2\pi\Delta f)$  in the scanning range  $\Delta f$  as

$$\varepsilon = 4\gamma(1 - \gamma) \left[ 1 - \frac{\sin^2(\pi\Delta f\tau)}{(\pi\Delta f\tau)^2} \right] \quad (18)$$

where  $\gamma$  is defined as the ratio of power in the slow eigenaxis to the total launched power

$$\gamma = \frac{1}{2}(1 + \hat{e}_s\hat{e}_f). \quad (19)$$

Fig. 4(a) and (b) shows the error signal given by (18) as a function of the signal frequency-scanning range-DGD product  $\Delta f\tau$  for different values of the power-splitting ratio  $\gamma$ . From Fig. 4(a), it is observed that the monotonicity of the error signal depends on the choice of the frequency-scanning range. For  $\Delta f\tau < 1$ , the error signal is monotonic, but it saturates for  $\Delta f\tau = 1$  and presents oscillations for  $\Delta f\tau > 1$ . For unambiguous control, we require  $\Delta f\tau \leq 1$ . From Fig. 4(b), it is observed that amplitude of the error signal is maximum for  $\gamma = 0.5$  and decreases for all other values of  $\gamma$ . The shape of the curves is independent of  $\gamma$ .

### III. EXPERIMENTAL SETUP

Fig. 5 shows the block diagram of the apparatus used for the experimental demonstration of the coherent frequency-selective polarimeter. A CW optical signal from a distributed feedback (DFB) semiconductor laser with wavelength 1559.79 nm was externally modulated using a Mach-Zender modulator (MOD)

<sup>4</sup>The most obvious choice is to assume that all spectral components have equal weights. Other weighting functions may be chosen instead, e.g., frequency components away from the center of the psd, which have less power and, therefore, are more affected by noise, could have smaller weights in (15).

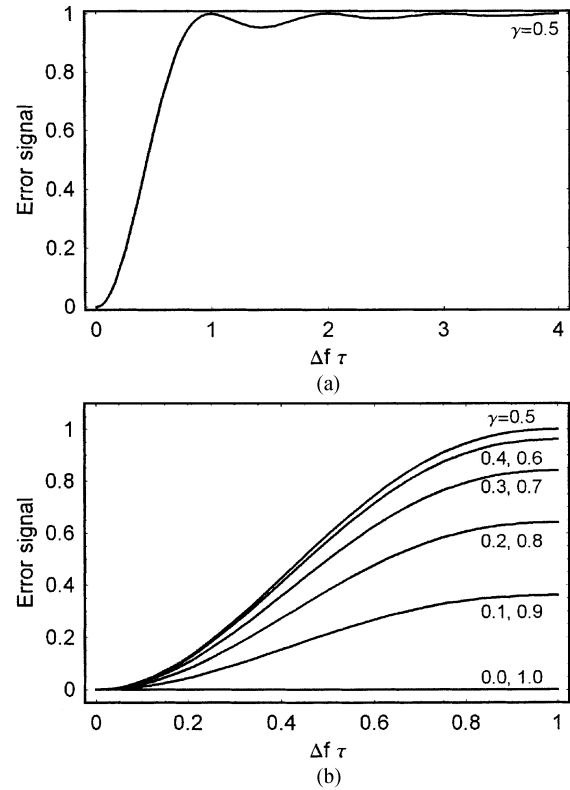


Fig. 4. Error signal given by (18) as a function of the frequency-scanning range-DGD product  $\Delta f\tau$  for different power splitting ratios. (a)  $\gamma = 0.5$  and (b)  $\gamma = 0-1$  with steps of 0.1 (curves corresponding to values of  $\gamma$  equidistant from 0.5 coincide).

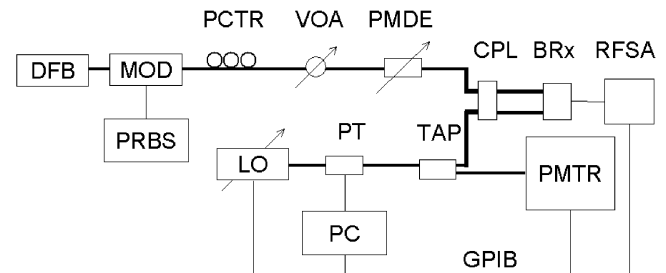


Fig. 5. Experimental setup for testing the proposed coherent frequency-selective polarimeter. DFB = distributed feedback semiconductor laser, MOD = Mach-Zender modulator, PRBS = pseudorandom bit sequence generator, PCTR = polarization controller, VOA = variable optical attenuator, PMDE = first-order PMD emulator, LO = local oscillator, PT = polarization transformer, PC = personal computer, TAP = 1% fiber tap, PMTR = polarimeter, CPL = 3-dB coupler, BRx = balanced receiver, RFSA = radio frequency spectrum analyzer, bold lines = optical fibers, and thin lines = electrical cables.

with nominally zero chirp. The bit rate was 10 Gb/s, the data format was NRZ, and the pseudorandom bit sequence (PRBS) period was  $2^{31} - 1$ . The optical signal passed through a manual polarization controller (PCTR), which was used to set the signal power-splitting ratio  $\gamma$  at the input of the first-order PMD emulator (PMDE). A variable optical attenuator (VOA) was used to adjust the optical power in the signal beam. A predetermined amount of DGD was introduced in the system using either a fixed length of PM fiber or a JDS (PE-3) first-order PMD emulator (PMDE). The optical signal at the input of the coherent receiver had an average power of  $-20$  dBm and an

optical signal-to-noise ratio (OSNR) of 40 dB, measured in a resolution bandwidth 0.1 nm. The local oscillator (LO) was an Agilent 8164F tunable laser module and was set to provide an average power at the receiver of  $-0.5$  dBm. The LO SOP was varied using an optoceramic polarization transformer (PT) (Corning Applied Technologies PC-412). Using a fiber tap (TAP), a small portion (1%) of the output of the polarization transformer was sent to a polarimeter (PMTR) (Agilent 8509C) in order to measure the Stokes parameters of the LO settings. The signal and LO beams passed through a 3-dB coupler (CPL) and into both input ports of a 750-MHz bandwidth-balanced receiver (BRx) (New Focus 1617). In the interest of system flexibility and ease of experimental implementation, the BPF, microwave mixer, and LPF of the coherent frequency-selective polarimeter, shown in the block diagram of Fig. 1(b), were emulated by a radio frequency spectrum analyzer (RFSA) (Anritsu MS2665C) in the experimental setup of Fig. 5. It was assumed that the resolution and video bandwidths of the radio-frequency (RF) spectrum analyzer correspond to the BPF and LPF equivalent noise bandwidths of the coherent frequency-selective polarimeter, respectively. A personal computer (PC) was used to send analog control voltages to the polarization transformer and to communicate with the LO laser, spectrum analyzer, and polarimeter via a general purpose interface bus (GPIB).

The experimental procedure for measuring Stokes parameters as a function of optical frequency was as follows: Before acquiring data, a calibration was first performed to determine four settings of the polarization transformer that created LO SOPs at roughly  $90^\circ$  intervals on the Poincaré sphere. It was not necessary to set the four LO SOPs precisely, since the algorithm for the evaluation of Stokes parameters only requires that the four LO SOPs are noncoplanar and known. In order to acquire data, the RF spectrum analyzer was set to operate in “zero span” mode, i.e., the center frequency of the BPF was fixed. The SOP of the LO was set to a given state using the polarization transformer. The carrier frequency of the LO was scanned across the optical channel at a fixed wavelength change rate of 500 pm/s (nominally 62 GHz/s). The signal at the output of the RF spectrum analyzer (referred to in the following as *RF psd*) was recorded into a file. The procedure was then repeated for a total of four LO SOP settings. The Stokes parameters of the LO SOP were also written into a file. Then, the algorithm of Section II-C was used to evaluate the frequency-resolved Stokes parameters.

It is worth noting here that fiber jumper cables connect the output of the transmission fiber and the LO with the polarization transformer, the 3-dB coupler, and the p-i-n photodiodes of the balanced receiver. The combined action of all fiber jumper cables alters the received signal and LO SOPs. However, it is assumed that all fiber jumper cables are short enough so their polarization-dependent loss (PDL) and PMD can be neglected. These assumptions imply that 1) the trajectory of the received signal SOP as a function of frequency is shifted on the Poincaré sphere, but its shape is not distorted and 2) the constellation of the four LO SOPs is rotated on the Poincaré sphere, but the relative positions of the points of the constellation are maintained. Therefore, the algorithm for the evaluation of the Stokes param-

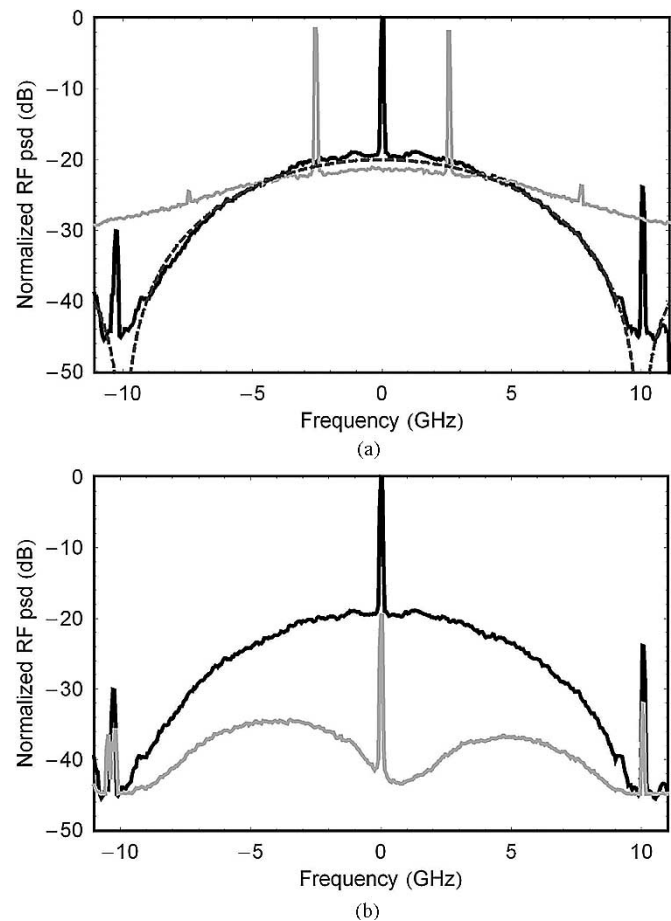


Fig. 6. (a) Sample RF psds, measured for two different values of the BPF center frequency,  $f_c \cong 0$  (black curve) and  $f_c = 2.5$  GHz (gray curve), in the absence of PMD. The theoretical psd of an ideal NRZ modulation is also shown (dashed curve) [20]. (b) Sample RF psds, measured in the absence of PMD (black curve) and in the presence of first-order PMD with nominal DGD equal to 40 ps (gray curve) for a BPF center frequency  $f_c \cong 0$  (conditions: resolution bandwidth  $B_{BPF} = 3$  MHz, video bandwidth  $B_{LPF} = 1$  kHz, scanning range  $\Delta f = 22$  GHz; no smoothing has been performed; all curves are normalized so the maximum RF power is 0 dBm).

eters of Section II-C can be applied. In addition, it was assumed that the position of the fiber jumpers does not change during the measurements due to environmental vibrations.

#### IV. EXPERIMENTAL RESULTS AND DISCUSSION

This section presents measurements, performed with the experimental setup of Section III, that demonstrate the successful operation of the coherent frequency-selective polarimeter. The impact of spectral folding on the performance of the proposed coherent frequency-selective polarimeter is thoroughly investigated.

Before proceeding to the main topic of this section, i.e., the measurement of the frequency-resolved Stokes parameters of a 10-Gb/s intensity-modulated NRZ optical signal, it is instructive to first visualize measured RF psds, which are distorted by spectral folding and PMD.

To illustrate the effect of spectral folding, Fig. 6(a) shows sample RF psds, measured for two different values of the BPF center frequency— $f_c \cong 0$  (black curve) and  $f_c = 2.5$  GHz (gray curve)—in the absence of PMD. Both curves are normal-

ized so that the maximum RF power is 0 dBm. The theoretical psd of an ideal NRZ modulation is also shown as the dashed curve [20]. It presents a central impulse (not included in the graph) due to the power transmitted at the signal carrier frequency and decreases proportionally to the inverse square of the frequency difference from the psd center [20]. The black curve exhibits the expected behavior, apart from the presence of small satellite spikes, separated by multiples of the bit rate, which are due to the nonideal (i.e., nonrectangular) shape of the NRZ pulses [20]. The 3-dB linewidth of all spikes, estimated to be several MHz, is due to the combined phase noise of the transmitter and LO. It is concluded that the effect of spectral folding *does not affect* the psd shape when  $f_c \cong 0$ . The operation of the coherent frequency-selective polarimeter is identical to the ideal case of  $f_c \gg R_b$ . In contrast, this is not the case when  $f_c$  becomes comparable to the bit rate  $R_b$ . For instance, in the case  $f_c = 2.5$  GHz, the RF psd shape is severely distorted (gray curve). There are two dramatic manifestations of spectral folding. First, it is observed that there are pairs of spikes around  $0, \pm 10, \pm 20, \dots$  GHz (only the first pair of spikes at  $\pm 2.5$  GHz and the innermost components of the second pair at  $\pm 7.5$  GHz are displayed in the graph). The spectral lines of each pair are separated by twice the BPF center frequency (i.e.,  $2f_c = 5$  GHz). These spurious spike pairs are generated when the intermediate frequency is swept and each spike of the total photocurrent psd passes consecutively through the positive and negative BPF passbands, respectively [see Fig. 3(b)]. Second, the side lobes of the gray curve are enhanced, as compared to the black curve, due to the overlap of psd segments centered at positive and negative intermediate frequencies within the BPF passband. We will examine below (Figs. 8 and 9) whether these psd distortions may affect the measurement of the Stokes parameters as well.

Study of Fig. 6(a) leads to the conclusion that both black and gray curves result from the addition of the powers of the spectral components at frequencies  $f_{IF} \pm f_c$ , in agreement with the empirical rule (4).

To illustrate the effect of PMD on the RF psd shape, Fig. 6(b) shows sample RF psds, measured in the absence (black curve) and in the presence of first-order PMD, with nominal DGD equal to 40 ps (gray curve), respectively, when  $f_c \cong 0$ . Both curves are normalized so that the maximum RF power is 0 dBm. It is observed that the effect of PMD is the scaling of the RF psd by a multiplication factor, which is a function of frequency and depends on the alignment of the signal and LO SOPs [see (35)]. In the case of first-order PMD, this multiplication factor varies sinusoidally as a function of frequency and its oscillation period is equal to the inverse of the DGD. Here, one of its troughs almost coincides with the central lobe of the RF psd and a spectral hole appears on the RF psd shape.

Fig. 7(a) and (b) show measured normalized Stokes parameters as a function of frequency (points) and their joint least-square error fitting by the set of functions (17) (solid lines) in the absence and in the presence of first-order PMD, respectively, when  $f_c \cong 0$ . A variant of the error signal defined by (15) was used as a metric for the fitting (referred to as *error function*). The error function was defined as the joint spectrally averaged standard deviation of the measured data from the

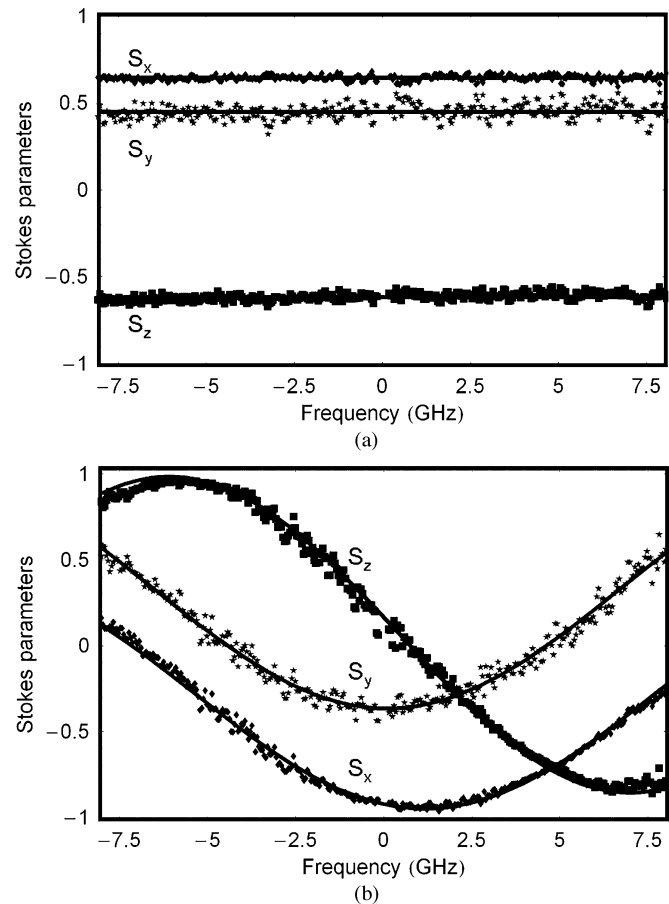


Fig. 7. Normalized Stokes parameters as a function of frequency (a) in the absence of PMD and (b) in the presence of first-order PMD with nominal DGD = 40 ps. Points=experimental data, solid lines = least-square error fitting by the set of functions (17). BPF center frequency  $f_c \cong 0$ , scanning range  $\Delta f = 16$  GHz. The rest of the RF spectrum analyzer settings were similar to Fig. 6).

fitting curves. It was evaluated assuming a uniform weighting function over the scanning range. In both Fig. 7(a) and (b), experimental results agree well with the theoretical prediction, confirming that the effect of spectral folding does not affect the measurement accuracy, at least for BPF center frequencies  $f_c \ll R_b$  [see (4)]. There are rapid small fluctuations of the measured Stokes parameters around the fitting curves, apparently due to the combined action of the noises in the coherent frequency-selective polarimeter. The joint spectrally averaged standard deviation of the measured data from the fitting curves is 5% in Fig. 7(a) and 6.5% in Fig. 7(b). It is worth mentioning that the estimate of DGD in Fig. 7(b), given by the least-square error fitting, is 38.2 ps, in good agreement with a Jones matrix eigenanalysis measurement [1] of the PM fiber coil (38.9 ps).

In order to study the impact of the BPF center frequency  $f_c$  on the performance of the coherent frequency-selective polarimeter, we repeated the measurements of Fig. 7 for BPF center frequencies  $f_c$  varying from 5 MHz up to 2.5 GHz. Figs. 8 and 9 show measured normalized Stokes parameters as a function of frequency (points) and their joint least-square error fitting by the set of functions (17) (solid lines) when  $f_c = 1$  GHz and  $f_c = 2.5$  GHz, respectively. In the absence of PMD [Figs. 8(a) and 9(a)], the measurement of the Stokes

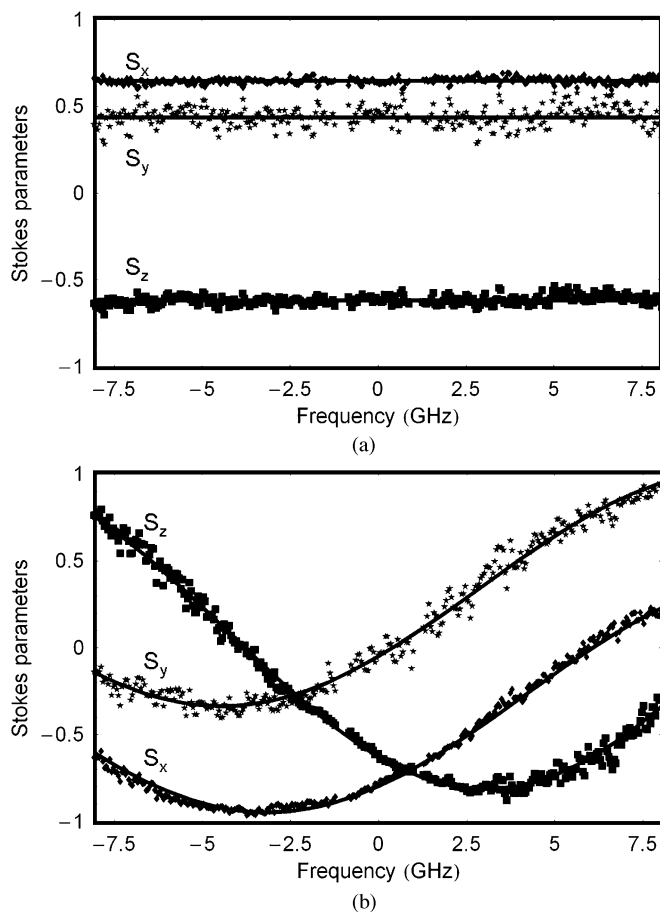


Fig. 8. Same as Fig. 7, for BPF center frequency  $f_c = 1$  GHz.

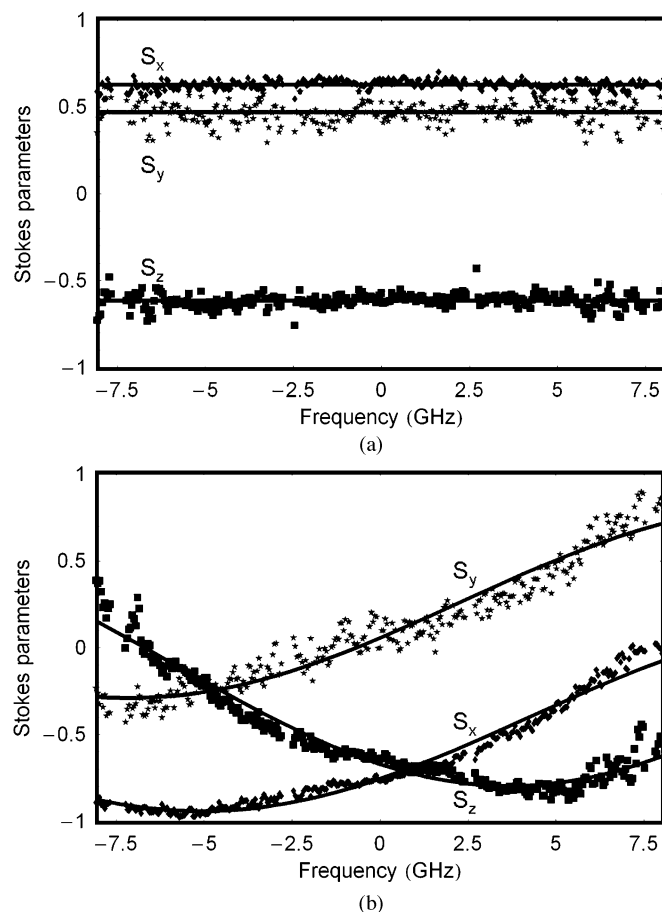


Fig. 9. Same as Fig. 7, for BPF center frequency  $f_c = 2.5$  GHz.

parameters is not affected by the choice of the BPF center frequency  $f_c$ . In the presence of first-order PMD [Figs. 8(b) and 9(b)], the goodness of fit deteriorates compared to the one displayed in Fig. 7(b). The joint spectrally averaged standard deviation of the measured data from the fitting curves in Figs. 8(b) and 9(b) is 6.9% and 11%, respectively. In addition, the estimate of DGD given by the least-square error fitting is 34.2 ps in Fig. 8(b) and 26.6 ps in Fig. 9(b), compared to 38.2 ps in Fig. 7(b), which is obviously wrong. This indicates that the set of functions (17) is not adequate for fitting when  $f_c\tau \geq 0.1$ , approximately, and that (14) should be used instead. We verified that there is indeed excellent agreement of the experimental data (points) in Figs. 8(b) and 9(b) and a theoretical fit of (14) (not shown in the figure in order to avoid clutter). It is worth noting that, for the latter fit, we used the same values of the parameters  $\alpha_k$ ,  $\beta_k$ ,  $k = x, y, z$ , and DGD as in 7(b). However, the phases  $\theta_k$ ,  $k = x, y, z$  were adjusted by an average of about  $57^\circ$  in Fig. 8(b) and of about  $65^\circ$  in Fig. 9(b), compared to the ones in Fig. 7(b). The physical mechanism that leads to this phase shift is not well understood.

Finally, to check the quality of the error signal generated by the coherent frequency-selective polarimeter, measurements of the Stokes parameters were made in the presence of first-order PMD with nominal DGD ranging from 0–100 ps (Fig. 10). The error signal was evaluated from the normalized Stokes parameters assuming a uniform weighting function and a scanning range of 10 GHz. As shown in Fig. 10, there is excellent agree-

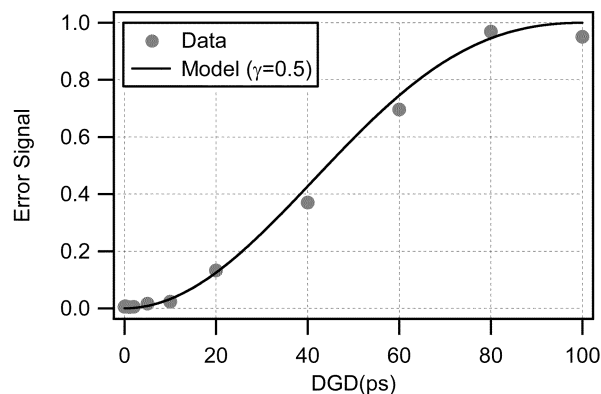


Fig. 10. Error signal versus DGD for a 10-Gb/s system. Points=measurements, line=expression (18) with  $\gamma = 0.5$ . Uniform weighting function, scanning range  $\Delta f = 10$  GHz; the rest of the RF spectrum analyzer settings were similar to Fig. 7.

ment of the experimental data (points) and a theoretical fit of (18) (solid line) for  $\gamma = 0.5$ .

All aforementioned measurements were performed with a resolution bandwidth equal to 3 MHz and a video bandwidth equal to 1 kHz. The performance of the proposed coherent frequency-selective polarimeter depends on the choice of BPF and LPF equivalent noise bandwidths. This dependence requires a detailed noise analysis, which will be reported in a separate paper.

## V. SUMMARY

In conclusion, we proposed and demonstrated a novel polarimeter based on coherent detection, which can resolve the Stokes parameters of a received modulated optical signal as a function of frequency with higher accuracy, compared to previously proposed direct detection-based counterparts.

It should be emphasized that the main purpose of the present paper was the proof of concept of the coherent frequency-selective polarimeter and not an exhaustive theoretical and experimental evaluation of its performance. Topics for future research should include a detailed study of the impact of noise on the performance of the coherent frequency-selective polarimeter, a comparison of error signals based on frequency-resolved Stokes parameters, and their use in adaptive PMD compensators.

## APPENDIX

This appendix presents a unified model of the frequency-selective polarimeters shown in Fig. 1. Analytical expressions for the output signal of both types of frequency-selective polarimeters are derived. Two received optical signal types are considered, i.e., CW and stochastic signals.

In the subsequent analysis, the following notations are used [23]: Dirac's bra and ket vectors denote Jones vectors, hats denote normalized Stokes vectors, and boldface letters denote electric field vectors. In addition, the analytic (i.e., phasor) and low-pass equivalent representations of bandpass signals and devices are used (see [20], ch. 4). These representations lead to elegant and concise mathematical expressions. For clarity, analytic signals are denoted by  $\circ$  and low-pass equivalent signals are denoted by a tilde in order to be distinguished from real signals. Finally, all noises and the effect of spectral folding are neglected.

1) *CW Signals*: The received electric field of a planar monochromatic wave can be written in analytic signal representation

$$\hat{\mathbf{E}}_{\mathbf{r}}(t) = \sqrt{2P_r} e^{i\omega_s t} |e_r\rangle \quad (20)$$

where  $P_r$  is the average power,  $\omega_s = 2\pi f_s$  is the carrier angular frequency, and  $|e_r\rangle$  is the SOP of the received optical signal.

Similarly, the electric field of the optical signal from the LO at the output of the polarization transformer can be written as

$$\hat{\mathbf{E}}_{\mathbf{l}_0}(t) = \sqrt{2P_{l_0}} e^{i\omega_{l_0} t} |e_{l_0}\rangle \quad (21)$$

where  $P_{l_0}$  is the average power,  $\omega_{l_0} = 2\pi f_{l_0}$  is the carrier angular frequency, and  $|e_{l_0}\rangle$  is the SOP of the optical signal from the LO at the output of the polarization transformer.

The electric fields at the output ports of an ideal, lossless, and polarization-independent 3-dB coupler are [25]

$$\begin{aligned} \hat{\mathbf{E}}_{\mathbf{r}_1}(t) &= \frac{1}{\sqrt{2}} \left[ \hat{\mathbf{E}}_{\mathbf{r}}(t) + i\hat{\mathbf{E}}_{\mathbf{l}_0}(t) \right] \\ \hat{\mathbf{E}}_{\mathbf{r}_2}(t) &= \frac{1}{\sqrt{2}} \left[ i\hat{\mathbf{E}}_{\mathbf{r}}(t) + \hat{\mathbf{E}}_{\mathbf{l}_0}(t) \right]. \end{aligned} \quad (22)$$

The photocurrent at the two branches of the balanced receiver is given by

$$i_k(t) = \frac{R_k}{2} \hat{\mathbf{E}}_{\mathbf{r}_k}^{\circ\dagger}(t) \cdot \hat{\mathbf{E}}_{\mathbf{r}_k}^{\circ}(t), \quad k = 1, 2 \quad (23)$$

where  $\dagger$  denotes the adjoint and  $R_{1,2}$  are the responsivities of the two photodiodes, respectively.

The total photocurrent results from the subtraction of the photocurrents at the two branches of the balanced receiver and can be calculated by (22) and (23). In the ideal case, when  $R_1 = R_2 = R$ , it is given by

$$i_{\text{tot}}(t) = i_1(t) - i_2(t) = R \Im \left[ \hat{\mathbf{E}}_{\mathbf{l}_0}^{\circ\dagger}(t) \cdot \hat{\mathbf{E}}_{\mathbf{r}}^{\circ}(t) \right] \quad (24)$$

where  $\Im[\cdot]$  denotes the imaginary part.

Substituting (20) and (21) into (24) yields

$$i_{\text{tot}}(t) = 2R\sqrt{P_r P_{l_0}} \Im \left[ \langle e_{l_0} | e_r \rangle e^{i\omega_{\text{IF}} t} \right] \quad (25)$$

where  $\omega_{\text{IF}} = \omega_s - \omega_{l_0} = 2\pi f_{\text{IF}}$ .

In the special case we consider now, there are signal spectral components only at  $\pm\omega_{\text{IF}}$ , so we set  $\omega_{\text{IF}} = \omega_c$ . Assuming, for simplicity, that the gain of the electronic preamplifier is unity and that the BPF transfer function presents negligible attenuation, the total photocurrent remains unchanged after the BPF, so  $i_{\text{BPF}}(t) = i_{\text{tot}}(t)$ .

The signal then passes through a microwave mixer, which is assumed to be an ideal square-law device. The signal at the output of the microwave mixer is the instantaneous electrical power  $P_e(t)$  on a unit resistor

$$P_e(t) = i_{\text{BPF}}^2(t).$$

$P_e(t)$  is comprised of discrete spectral components at frequencies  $f = 0$  and  $\pm 2f$ . In the special case under study, the sole purpose of the LPF is to eliminate the higher harmonic at  $\pm 2f_c$  at the output of the microwave mixer. The bandwidth of the LPF is not critical as long as  $B_{\text{LPF}} \ll 2f_c$ . After the LPF, only the direct current (dc) spectral component survives, so the output signal of the coherent frequency-selective polarimeter is the average electrical power on a unit resistor

$$\bar{P}_e = 2R^2 P_r P_{l_0} |\langle e_{l_0} | e_r \rangle|^2. \quad (26)$$

It is straightforward to show that the photocurrent at the output of the frequency-selective polarimeter of Fig. 1(a), based on direct detection, is given by a similar expression

$$i_{\text{dd}} = R P_r |\langle e_{\text{pol}} | e_r \rangle|^2 \quad (27)$$

where  $|e_{\text{pol}}\rangle$  is a normalized Jones vector denoting the eigenaxis of the polarizer.

2) *Stochastic Signals*: In this section, we extend the previous mathematical description to the case of a modulated transmitted optical signal. The modulating signal is assumed to be a sample function of a wide-sense stationary stochastic process. The electric field of the LO is, again, described by (21).

The electric field of the optical signal at the output of the transmitter can be written in analytic signal representation as

$$\hat{\mathbf{E}}_{\mathbf{s}}(t) = \sqrt{P_s} \tilde{d}(t) e^{i\omega_s t} |e_s\rangle \quad (28)$$

where  $\tilde{d}(t)$  is the complex envelope of the random modulating signal with unit average power.

It is assumed that transmission through the optical fiber introduces attenuation, chromatic dispersion, and PMD. For simplicity, PDL and all fiber nonlinearities are neglected. Although these assumptions are not always valid, they allow for a succinct mathematical description of frequency-selective polarimeters. Due to their linear nature, the action of attenuation, chromatic dispersion, and PMD can be separated.

The received optical power is

$$P_r = e^{-aL} P_s \quad (29a)$$

where  $a$  is the attenuation coefficient and  $L$  is the length of the optical fiber.

The action of the chromatic dispersion can be modeled as a lossless all-pass filter with impulse response [26]

$$\tilde{h}_f(t) = \frac{1}{\sqrt{2\pi i \beta_2 L}} e^{-\frac{t^2}{2i\beta_2 L}}$$

where  $\beta_2$  is the group velocity dispersion (GVD) coefficient at the signal carrier frequency. We neglected the phase shift and group delay introduced by the optical fiber.

Chromatic dispersion alters the complex envelope of the modulating signal

$$\tilde{g}(t) = \tilde{d}(t) \otimes \tilde{h}_f(t) \quad (29b)$$

where  $\otimes$  denotes convolution. Due to the lossless all-pass nature of  $\tilde{h}_f(t)$ , the (unit) average power is preserved in (29b).

Due to the PMD of the optical fiber, the input and output Jones vectors are related through the expression (in the frequency domain) [23]

$$|e_r(f)\rangle = \tilde{U}(f)|e_s\rangle \quad (29c)$$

where  $\tilde{U}(f)$ , in the absence of PDL, is a unitary operator denoting the low-pass equivalent polarization transfer function of the fiber [23].

Combining (29a)–(29c), the electric field of the received optical signal can be written as

$$\overset{\circ}{\mathbf{E}}_r(t) = \sqrt{P_r} \tilde{g}(t) \otimes |e_r(t)\rangle e^{i\omega_s t} \quad (30)$$

where  $|e_r(t)\rangle$  is a *nonnormalized* Jones vector describing the SOP of the received optical signal as a function of time

$$|e_r(t)\rangle = \int_{-\infty}^{\infty} |e_r(f)\rangle e^{i\omega t} df.$$

Repeating the calculations of the previous section, it is straightforward to show that the total photocurrent can be written as

$$i_{\text{tot}}(t) = R\sqrt{2P_r P_{10}} \Im \{ \tilde{g}(t) \otimes \langle e_{10} | e_r(t) \rangle e^{i\omega_{\text{IF}} t} \}. \quad (31)$$

The analytic signal representation of the total photocurrent is

$$\overset{\circ}{i}_{\text{tot}}(t) = -iR\sqrt{2P_r P_{10}} \tilde{g}(t) \otimes \langle e_{10} | e_r(t) \rangle e^{i\omega_{\text{IF}} t}. \quad (32)$$

The autocorrelation of (32) is [20]

$$\phi_{\overset{\circ}{i}_{\text{tot}}}( \tau ) \equiv \frac{1}{2} E \left\{ \overset{\circ}{i}_{\text{tot}}^*(t - \tau) \overset{\circ}{i}_{\text{tot}}(t) \right\} \quad (33)$$

where  $E\{\cdot\}$  denotes the expected value (ensemble average) and  $*$  denotes the complex conjugate.

The one-sided psd of the total photocurrent is the Fourier transform of (33) [20]

$$\Phi_{\overset{\circ}{i}_{\text{tot}}}(f) \equiv \int_{-\infty}^{\infty} \phi_{\overset{\circ}{i}_{\text{tot}}}( \tau ) e^{-i\omega \tau} d\tau. \quad (34)$$

Substituting (32) and (33) into (34) yields

$$\Phi_{\overset{\circ}{i}_{\text{tot}}}(f) = 2R^2 P_r P_{10} |\langle e_{10} | e_r(f - f_{\text{IF}}) \rangle|^2 \Phi_{\tilde{g}}(f - f_{\text{IF}}) \quad (35)$$

where  $\Phi_{\tilde{g}}(f)$  is the psd of the modulating signal  $\tilde{g}(t)$ .

Assuming, for simplicity, that the gain of the electronic preamplifier is unity, the one-sided psd of the photocurrent at the output of the BPF is

$$\Phi_{\overset{\circ}{i}_{\text{BPF}}}(f) = \Phi_{\overset{\circ}{i}_{\text{tot}}}(f) \left| \overset{\circ}{H}_{\text{BPF}}(f) \right|^2 \quad (36)$$

where  $\overset{\circ}{H}_{\text{BPF}}(f)$  is the analytic signal representation of the BPF transfer function.

As explained qualitatively in Fig. 2, due to the finite BPF bandwidth, the signal at the output of the BPF has amplitude modulation resulting from the presence of spectral components adjacent to the center frequency of the BPF. This amplitude modulation creates fluctuations at the output of the coherent frequency-selective polarimeter (i.e., data noise). Additional output fluctuations are created by the thermal and shot noise of the coherent receiver front-end, as well as the filtering of the transmitter and LO phase noise by the BPF.

The purpose of the LPF in the case under study is two-fold: 1) to eliminate the second harmonic at  $\pm 2f_c$  at the output of the microwave mixer, i.e.,  $B_{\text{LPF}} \ll 2f_c$  and 2) average the amplitude variations due to the data, shot, thermal, and phase noise after the BPF. This averaging is not perfect, so the output of the coherent frequency-selective polarimeter varies over time, i.e.,  $\overline{P}_e(t)$ . The expected value of the output is

$$\begin{aligned} E \{ \overline{P}_e(t) \} &= \frac{1}{2} \int_{-\infty}^{\infty} E \left\{ \left| \overset{\circ}{i}_{\text{BPF}}(t - \xi) \right|^2 \right\} h_{\text{LPF}}(\xi) d\xi \\ &= H_{\text{LPF}}(0) \phi_{\overset{\circ}{i}_{\text{BPF}}}(0) \end{aligned} \quad (37)$$

where  $h_{\text{LPF}}(t)$  and  $H_{\text{LPF}}(f)$  are the impulse response and transfer function of the LPF, respectively, and  $\phi_{\overset{\circ}{i}_{\text{BPF}}}( \tau )$  is the autocorrelation of the analytic signal representation of the photocurrent at the output of the BPF

$$\phi_{\overset{\circ}{i}_{\text{BPF}}}( \tau ) = \int_{-\infty}^{\infty} \Phi_{\overset{\circ}{i}_{\text{BPF}}}(f) e^{i\omega \tau} df. \quad (38)$$

It is assumed that the BPF is narrow enough so that the terms  $|\langle e_{10} | e_r(f - f_{\text{IF}}) \rangle|^2$  and  $\Phi_{\tilde{g}}(f - f_{\text{IF}})$  in (35) do not vary significantly within the BPF passband as a function of frequency. Consequently, it is possible to expand  $|\langle e_{10} | e_r(f - f_{\text{IF}}) \rangle|^2$  and

$\Phi_g(f - f_{IF})$  in Taylor series about  $f_c$  and retain only the first (i.e., zero-order) term. The substitution of (35) and (36) into (38) yields

$$\phi_{i_{BPF}}(0) \cong 2R^2 P_s P_{Io} \left| \overset{\circ}{H}_{BPF}(0) \right|^2 \times |\langle e_{Io} | e_r(f_c - f_{IF}) \rangle|^2 \Phi_{\tilde{g}}(f_c - f_{IF}) B_{BPF} \quad (39)$$

where  $B_{BPF}$  is the BPF equivalent noise bandwidth defined as [20]

$$B_{BPF} \equiv \frac{\int_{-\infty}^{\infty} \left| \overset{\circ}{H}_{BPF}(f) \right|^2 df}{\left| \overset{\circ}{H}_{BPF}(0) \right|^2} = \frac{\int_{-\infty}^{\infty} \left| \tilde{H}_{BPF}(f) \right|^2 df}{\left| \tilde{H}_{BPF}(0) \right|^2} \quad (40)$$

where  $\tilde{H}_{BPF}(f)$  is the low-pass equivalent representation of the BPF transfer function.

From (39), (37) is written for lossless BPF, LPF as

$$E \{ \bar{P}_e(t) \} \cong 2R^2 P_s P_{Io} |\langle e_{Io} | e_r(f_c - f_{IF}) \rangle|^2 \times \Phi_{\tilde{g}}(f_c - f_{IF}) B_{BPF}. \quad (41)$$

It is straightforward to show that the expected value of the photocurrent at the output of frequency-selective polarimeters based on direct detection is given by a similar expression

$$E \{ i_{dd}(t) \} \cong R P_r |\langle e_{pol} | e_r(f_c - f_s) \rangle|^2 \Phi_{\tilde{g}}(f_c - f_s) B_o \quad (42)$$

where  $B_o$  is the equivalent noise bandwidth of the tunable optical filter.

It should be stressed that (42) is valid only when  $|\langle e_{pol} | e_r(f - f_s) \rangle|^2$  and  $\Phi_{\tilde{g}}(f - f_s)$  do not vary significantly within the passband of the tunable optical filter as a function of frequency. However, practical tunable optical filters are wide enough ( $\sim$  GHz), so this assumption is not valid and higher order terms in the Taylor series must be retained. These higher order terms lead to a systematic error in the output signal of frequency-selective polarimeters based on direct detection. Deconvolution with the transfer function of the tunable optical filter is then necessary in order to reduce the systematic error [4]. Such deconvolution is unnecessary for the proposed coherent frequency-selective polarimeter, due to the narrowband electronic BPFs ( $\sim$  MHz bandwidth). In conclusion, the coherent frequency-selective polarimeter has smaller systematic error compared to previously proposed direct-detection-based counterparts.

#### ACKNOWLEDGMENT

The authors would like to thank Drs. R. S. Vodhanel and D. Pikula for helpful discussions and the anonymous reviewers for their comments and suggestions.

#### REFERENCES

[1] C. D. Poole and J. Nagel, "Polarization effects in lightwave systems," in *Optical Fiber Telecommunications*, I. P. Kaminow and T. L. Koch, Eds. San Diego, CA: Academic, 1997, vol. III-A, ch. 6, pp. 114–161.

[2] E. Brinkmeyer, "PMD compensation," in *Proc. Eur. Conf. Optical Commun. (ECOC'02)*, Copenhagen, Denmark, Sept. 2002, paper 9.3.1.

[3] H. Rosenfeldt, R. Ulrich, U. Feiste, R. Ludwig, H. G. Weber, and A. Ehrhardt, "PMD compensation in 10 Gbit/s NRZ field experiment using polarimetric error signal," *Electron. Lett.*, vol. 36, no. 5, pp. 448–450, 2000.

[4] L. Möller and L. Buhl, "Method for PMD vector monitoring in picosecond pulse transmission systems," *J. Lightwave Technol.*, vol. 19, pp. 1125–1129, 2001.

[5] P. Westbrook, L. Möller, S. Chandrasekhar, R. Dutta, and S. Wielandy, "Wavelength sensitive polarimeter for multichannel polarization and PMD monitoring," in *Proc. Optical Fiber Communication Conf. (OFC'02)*, Anaheim, CA, Mar. 2002, paper WK5.

[6] I. Roudas, G. Piech, M. Mlejnek, Y. Zhu, and D. Q. Chowdhury, "Coherent heterodyne frequency-selective polarimeter for error-signal generation in higher-order PMD compensators," in *Proc. Optical Fiber Communication Conf. (OFC'02)*, Anaheim, CA, Mar. 2002, paper WQ2.

[7] R. A. Linke and A. H. Gnauck, "High-capacity coherent lightwave systems," *J. Lightwave Technol.*, vol. 5, pp. 1750–1769, Nov. 1988.

[8] A. Papoulis and S. U. Pillai, *Probability, Random Variables and Stochastic Processes*, Fourth ed. New York: McGraw-Hill, 2002, ch. 12.

[9] D. M. Baney, B. Szafraniec, and A. Motamedi, "Coherent optical spectrum analyzer," *IEEE Photon. Technol. Lett.*, vol. 14, pp. 355–357, Mar. 2002.

[10] B. Szafraniec, A. Motamedi, and D. M. Baney, "Polarization-diverse coherent optical spectrum analyzer with swept local oscillator," in *Proc. Optical Fiber Communication Conf. (OFC'02)*, Anaheim, CA, Mar. 2002, paper ThGG5.

[11] G. D. VanWiggeren, A. R. Motamedi, B. Szafraniec, R. S. Tucker, and D. M. Baney, "Single-scan polarization-resolved heterodyne optical network analyzer," in *Proc. Optical Fiber Communication Conf. (OFC'02)*, Anaheim, CA, Mar. 2002, paper WK2.

[12] J. S. Bendat and A. G. Piersol, *Random Data: Analysis and Measurement Procedures*, Second ed. New York: Wiley, 1986.

[13] O. K. Tonguz, O. M. Tanrikulu, and L. G. Kazovsky, "Performance of coherent ASK lightwave systems with finite intermediate frequency," *IEEE Trans. Commun.*, vol. 45, pp. 344–351, Mar. 1997.

[14] B. S. Glance, "An optical heterodyne mixer providing image-frequency rejection," *J. Lightwave Technol.*, vol. LT-4, pp. 1722–1725, Nov. 1986.

[15] F.-J. Westphal and B. Strebler, "Optical heterodyne image rejection receiver," *Electron. Lett.*, vol. 24, pp. 440–442, Mar. 1988.

[16] T. Chikama, T. Naito, S. Watanabe, T. Kiyonaga, M. Suyama, and H. Kuwahara, "Optical heterodyne image-rejection receiver for high-density optical frequency division multiplexing system," *IEEE J. Select. Areas Commun.*, vol. 8, pp. 1087–1094, Aug. 1990.

[17] G. P. Agrawal, *Fiber-Optic Communication Systems*, Second ed. New York: Wiley, 1992.

[18] J. G. Proakis and D. G. Manolakis, *Digital Signal Processing: Principles, Algorithms and Applications*, Third ed. Englewood Cliffs, NJ: Prentice-Hall, 1996.

[19] K. S. Shanmugam, *Digital and Analog Communication Systems*. New York: Wiley, 1979.

[20] J. G. Proakis, *Digital Communications*, Third ed. New York: McGraw-Hill, 1995.

[21] M. Born and E. Wolf, *Principles of Optics*, Sixth ed. New York: Cambridge Univ. Press, 1997.

[22] S. Shin, I. Yeo, H. Song, J. Park, Y. Park, and B. Jo, "Real-time endless polarization tracking and control system for PMD compensation," in *Proc. Optical Fiber Communication Conf. (OFC'01)*, Anaheim, CA, Mar. 2001, paper TuP7.

[23] J. P. Gordon and H. Kogelnik, "PMD fundamentals: Polarization mode dispersion in optical fibers," *Proc. Nat. Acad. Sci.*, vol. 97, no. 9, pp. 4541–4550, 2000.

[24] R. M. A. Azzam, I. M. Elminyawi, and A. M. El-Saba, "General analysis and optimization of the four-detector photopolarimeter," *J. Opt. Soc. Amer. A*, vol. 5, no. 5, pp. 681–689, 1988.

[25] G. L. Abbas, V. W. S. Chan, and T. K. Yee, "A dual-detector optical heterodyne receiver for local oscillator noise suppression," *J. Lightwave Technol.*, vol. LT-3, pp. 1110–1122, 1985.

[26] L. G. Kazovsky, S. Benedetto, and A. Willner, *Optical Fiber Communication Systems*. Boston, MA: Artech, 1996.

[27] D. Q. Chowdhury, I. Roudas, and R. S. Vodhanel, "System and method for measurement of the state of polarization over wavelength," U.S. Patent 6 563 590, May 13, 2003.

**I. Roudas** received the B.S. degree in physics and the M.S. degree in electronics and radio engineering from the University of Athens, Athens, Greece, in 1988 and 1990, respectively, and the M.S. and Ph.D. degrees in coherent optical communication systems from the Ecole Nationale Supérieure des Télécommunications, Paris, France, in 1991 and 1995, respectively.

From 1995 to 1998, he was with the Optical Networking Research Department, Bell Communications Research (Bellcore), Red Bank, NJ. In addition, he was an Adjunct Professor of the graduate course entitled "Lightwave Systems" at the Electrical Engineering Department, Columbia University, New York, NY, during the fall semesters of 1997 and 1998. From 1999 to 2002, he was with the Photonic Modeling and Process Engineering Department, Corning Incorporated, Somerset, NJ. He recently joined the Department of Electrical and Computer Engineering, University of Patras, Patras, Greece, as an Associate Professor of optical communications. He is the author or coauthor of more than 40 papers in scientific journals and international conferences and holds two patents.

Dr. Roudas serves as a Reviewer for the *IEEE/OSA JOURNAL OF LIGHTWAVE TECHNOLOGY*, the *IEEE PHOTONICS TECHNOLOGY LETTERS*, and *Optics Communications*.

**G. A. Piech** received the B.A. degree in physics from Dartmouth College, Hanover, NH, in 1992 and the Ph.D. degree from the University of Wisconsin, Madison, in 1998. His Ph.D. dissertation involved the study of electron collisions with metastable atoms using optical methods.

In 1998, he joined Mission Research Corporation, Los Angeles, CA, where he worked on developing novel laser radar technologies. In 2000, he joined Corning, Inc., Corning, NY, working on polarization-mode dispersion measurements and compensation techniques. His current research interests include low noise and coherent detection techniques, precision spectroscopic measurements, and optical system design.

**M. Mlejnek** graduated from Charles University, Prague, Czech Republic, and received the Ph.D. degree in optics from the University of Arizona, Tucson.

He also was a Postdoctoral Fellow at the University of Arizona before joining Corning, Inc., Corning, NY. He is currently a Senior Research Scientist in the Science and Technology Division. In the course of his career, he has conducted theoretical investigations in the areas of short optical pulse interaction with nonlinear and linear media, such as semiconductors and air, and the generation of terahertz ultrashort pulses. His continuing interest involves liquid-crystal displays, imaging, atmospheric propagation, chromatic and polarization dispersion compensation, and information theory.

**Y. Mauro** received the B.E. degree from Shanghai Jiaotong University, Shanghai, China, the M.E. degree from Huazhong University of Science and Technology, Wuhan, China, and the M.A.S. degree from the University of Ottawa, Ottawa, ON, Canada, all in electrical engineering.

She joined the Research and Development Department, Corning, Incorporated, Corning, NY, in 1999 as a Senior Research Scientist. Her research interests include optical communication, liquid-crystal displays, nonlinear optics, polarization dispersion compensation, and optical systems and devices modeling.

**D. Q. Chowdhury** (S'89–M'89) received the B.Sc. degree in electrical engineering from Bangladesh University of Engineering and Technology, Dhaka, Bangladesh, in 1986 and the M.S. and Ph.D. degrees in electrical engineering from Clarkson University, Potsdam, NY, in 1989 and 1991, respectively.

From 1991 to 1993, he had a joint appointment as a Research Associate in the Applied Physics Department, Yale University, New Haven, CT, and in the Electrical Engineering Department, New Mexico State University, Las Cruces, NM. For his graduate and postgraduate work, he performed numerical modeling of, and experimentation on, optical scattering from nonlinear microcavities. He joined the research and development facility of Corning, Inc., Corning, NY, in 1993. Since joining Corning, he has focused his research efforts on various aspects of optical communication systems. Currently, he is Research Director of Modeling and Simulation, managing optical system and device modeling and general process modeling for Corning Research. His research interests include linear and nonlinear devices; impairments in fiber-optic systems and networks, e.g., nonlinearities, crosstalk, chromatic dispersion, and polarization-mode dispersion; and efficient algorithms for simulating fiber-optic systems.

**M. Vasilyev** (S'98–M'99) received the M.S. degree in physics from the Moscow Institute of Physics and Technology, Moscow, Russia, in 1993 and the Ph.D. degree in electrical engineering from Northwestern University, Evanston, IL, in 1999.

His research at Lebedev Physics Institute, Moscow, Russia, from 1993 to 1994 and doctoral work at Northwestern were on the quantum properties of novel optical amplifiers and solitons in optical fibers. He joined the Photonic Research and Test Center, Corning, Inc., Somerset, NJ, as a Senior Research Scientist in 1999, where he has been studying noise and nonlinearities in Raman amplifiers and erbium-doped fiber amplifiers (EDFAs), as well as fiber-transmission issues and other impairments in dense wavelength division multiplexing (WDM) systems and networks. He is the author or coauthor of more than 60 journal and conference papers.

Dr. Vasilyev is a Member of the IEEE Lasers and Electro-Optics Society, the IEEE Communication Society, and the Optical Society of America, currently serving on the Technical Program Committee for the Optical Amplifiers and their applications conference.